Ceramics International 49 (2023) 33445–33458

Contents lists available at ScienceDirect

Ceramics International

journal homepage: www.elsevier.com/locate/ceramint

Effect of sintering temperature on microstructure, optical and dielectric properties in a low radio frequency range of a BaO:ZnO composite

Muhammad Haseeb [a], Muneeb Irshad [b], Mohsin Saleem [c,d], Abid Aleem [e], Muhammad Arshad [f], Atif Shahbaz [a], Muhammad Imran [a], Rabia Ghaffar [g], Hafiz Ahmad Ishfaq [h,i], Abdul Ghaffar [a,*]

[a] Department of Physics, Government College University, Lahore, 54000, Pakistan
[b] Department of Physics, University of Engineering and Technology, Lahore, 54890, Pakistan
[c] School of Chemical and Materials Engineering (SCME), National University of Sciences and Technology (NUST), Islamabad, Pakistan
[d] School of Interdisciplinary Engineering & Sciences, National University of Sciences and Technology (NUST), Islamabad, Pakistan
[e] RF Acceleration Group, LINAC Project, PINSTECH, P. O. Box Nilore, Islamabad, 45650, Pakistan
[f] Nanosciences & Technology Department, National Center for Physics, Quaid-i-Azam University Campus, Islamabad, Pakistan
[g] Division of Science and Technology, Department of Botany, University of Education, Lahore, 54000, Pakistan
[h] Department of Materials Chemistry, National Institute of Chemistry, Hajdrihova 19, 1000, Ljubljana, Slovenia
[i] Faculty of Chemistry and Chemical Technology, University of Ljubljana, Večna Pot 113, 1000, Ljubljana, Slovenia

ARTICLE INFO

Handling Editor: Dr P. Vincenzini

Keywords:
BaO:ZnO ceramic composite
Sintering
Dielectric measurements
Low radio frequency range of 0.0–2.0MHz
Stability of dielectric character

ABSTRACT

Effect of sintering, between 550 and 950 °C, on dielectric properties of ceramic composite BaO:ZnO (BZO) was investigated in a low radio frequency range of 0.0–2.0 MHz. BZO ceramic composite was prepared by the facile autocombustion synthesis method. BaO and ZnO crystallized into tetragonal and hexagonal structures, respectively, coexist as an agglomerated microstructure inside the BZO composite. UV–Vis DRS, FTIR, photoluminescence and Raman spectroscopy were employed to find band gap energies, functionalization groups, excitation wavelength and the presence of vibrational modes of the sintered BZO composites. Scanning electron microscopy sufficed agglomerated structure of increasing particle size with temperature. Dielectric analysis showed that the maximum dielectric constant of 1.8 was observed for the composite sintered at 550 °C and then it decreased after heating at 650 °C. On further heating, an increase was observed in the dielectric constant of the BZO till 950 °C. The initial decrease was attributed to the presence of residual $Ba(OH)_2$ phase. The loss tangent was reduced from 0.6 to 0.02 due to the post-synthesis sintering process. The sintered BZO exhibited increase in conductivity and decrease in resistivity in 0.0–2.0 MHz range. Similarly, the overall decline in real and imaginary permittivity was noticed with a uniform trend in the limit of 0.5–2.0 MHz. An increase in crystallite size from 41.36 to 92.54 nm for BaO and 22.23 to 40.99 nm for ZnO affected the dielectric constant. First, it decreased after heating at 650 °C and then increased up to 950 °C. During heating, a decrease in the interfacial polarization and an increase in the ionic polarization were attributed to the inter- and intra-crystallite boundary variations that played a role in the overall dielectric character of the BZO. The stability of dielectric parameters in the 0.25–2.0 MHz range suggested tuning these quantities by simply sintering process.

1. Introduction

Dielectric materials [1] as an essential part of electrical energy storage devices are being integrated in many electrical appliances and gadgets in our daily life, particle beam accelerators for high-energy applications, high-power microwave generators [2–4] and the electric automobile industry. The bigger challenge with capacitors that require a dielectric medium is to enhance their energy density with an appropriate compromise with the power density [5]. As per the nature of capacitor assembly, the air-breakdown effect can be reduced by tuning the dielectric properties of the medium between the plates, for example, by introducing poly(vinylidene fluoride) in barium titanate to change its permittivity [6]. Regarding the processing and measuring, the dielectric properties of materials [7] strongly affected by heat treatment, heating method, thermal characteristics of the dielectric material and heating rate [8,9]. Materials are also being studied for their dielectric response in high-frequency regimes with minimum losses (so called loss tangent)

* Corresponding author.
E-mail address: abdulghaffar@gcu.edu.pk (A. Ghaffar).

https://doi.org/10.1016/j.ceramint.2023.06.069
Received 18 April 2023; Received in revised form 21 May 2023; Accepted 8 June 2023
Available online 9 June 2023
0272-8842/© 2023 Elsevier Ltd and Techna Group S.r.l. All rights reserved.

Symbols

BaO	ZnO as BZO
a	and c as lattice parameters
d	as interplanar spacing
D	as crystallite size
E_g	as band gap energy
ε'	as dielectric constant
C_p	as specific capacitance
Z	as impedance
ε	as permittivity
tanδ	as loss tangent

[10,11]. Similarly, the dielectric nature of the ceramics considered in the microwave limits strongly depends upon the precursor materials, processing (synthesis) and densification of the internal micro- or nano-structure due to certain heat treatment [12]. In the list of dielectric materials, mixed metal oxide ceramics are also being investigated as they show synergistic dielectric character coming from phases involved [13,14].

Zn and Ba-based metal oxide composites are revealing excellent electronic and dielectric properties [15,16]. Since the present study focused on barium oxide (BaO) and zinc oxide (ZnO) in the composite form. Both BaO and ZnO are not commonly known as dielectric materials. But they reveal notable electrical and dielectric properties when used in composite or doped forms with other metals and metal oxides-based materials [17,18]. Few studies have been carried out on the BaO–ZnO and discussed its electrical, ferroelectric and dielectric characteristics. For example, the variable resistance of ZnO–BaO 5 mol% barium oxide prepared at a different temperature from 900 to 1350 °C by liquid mix technique was evaluated. A minima and maxima in the loss factor have been observed at 8 kHz and 12 kHz, respectively, whereas the maximum loss factor is due to the interfacial polarization [19]. Due to the solubility of BaO in water, the applications of ZnO/BaO are limited, similar to ZnO/Bi_2O_3. However, still, it is used to fabricate varistors [20]. Nonohmic behavior is seen in the same binary ZnO/BaO due to the nonlinearity in the voltage-current nature due to the irregular and non-uniform presence of the BaO around the ZnO grains [21]. Ferroelectric and dielectric investigations of ZnO/BaO nanofibers sufficed a dielectric constant of 132 at 323 °C and 800 Hz. Moreover, the dielectric studies showed that ZnO/BaO composite exhibit a ferroelectric to paraelectric phase transition at 323 K [22].

Zn, Ba and their oxides have been considered part of other materials and revealed remarkable dielectric results. The combination of different materials can lead to enhance dielectric properties of new materials regarding certain technological significance [23,24] as also seen in the case of carbon-based composites with improved electronic features [25,26]. For well-known $PbO–ZnO–B_2O_3$ glass, when BaO replaces PbO, the thermal expansion gets better for the sintering range of 550 to 580 °C [27]. Similarly, atomic layer deposition of barium oxide mixed with titanium oxide showed large dielectric constant values [28]. Zn and Ba as an integrated mixture phase of $BaSrZnTiO_3$ ceramic material exhibit ferroelectric behavior and dielectric properties at 40 Hz - 1 MHz [29,30]. ZnO composite with the polymer (polyvinyl alcohol) has been investigated as a thin film, revealing good dielectric properties as a function of frequency [31,32]. Likewise, when subjected to external pressure, ZnO nanowires randomly integrated into porous polydimethylsiloxane, an elastomer, lead to the variation of the dielectric constant and permittivity necessary for the detection purposes (sensors) in terms of capacitance variations [33]. $BaTiO_3$ doped with ZnO enhances the permittivity and dielectric properties during the sintering with reduced dielectric losses [34], making it useful for high-field fast signal transmission [35]. Similar properties have also been achieved simply by Zn doping in PVDF (poly(vinylidene fluoride)) as a candidate for capacitor applications [36]. Composite particles of polystyrene and ZnO in the form of suspension have been investigated in the range of 40 Hz–110 MHz. This offers to explore the influence of volume fraction and concentration of polystyrene/ZnO particles on the dielectric properties [37].

Along with the dielectric materials with large dielectric constants that offer increased electronic flow restriction [38,39], there are low dielectric ceramic glasses such as SiO_2 glass and $SiO_2–B_2O_3–Al_2O_3–BaO–ZrO_2$ with a dielectric constant 4.0–4.8 [40]. The dielectric constant can easily be reduced by increasing the amount of one of the constituents of the ceramic composite. For example, by increasing the amount of Mg_2TiO_4 from 50 wt% to 80 wt%, the dielectric constant of $Ba_{0.5}Sr_{0.5}TiO_3–Mg_2TiO_4$ is reduced to 35 from 335 [41]. The dielectric properties can also be varied via a sintering process that reduces the pore volume and enhances the polarization phenomenon [42,43].

Various studies on the dependence of the dielectric nature of materials on the sintering temperature have been reported. As Sn- and Cu-based ferrite nanoparticles sintered at 300 °C, 600 °C, and 900 °C revealed modification of the dielectric constant in 100 KHz - 700 MHz [44]. Nanosilica after the 75 MPa uniaxial applied pressure gone through the sintering process at 1330, 1360, 1390, 1420, and 1450 °C for 2 h. The effect of sintering is translated in terms of a maximum dielectric constant of 544.28 with a dielectric loss of 195.94 [45]. The temperature-induced dielectric character of $Bi_4NdTi_3FeO_{15}$ produces dielectric relaxation which is attributed to the short-range dynamics of the oxygen vacancies [46]. Similarly, forsterite (Mg_2SiO_4) ceramic exhibits a small variation in the dielectric constant while sintered in the range of 1250–1450 °C [47]. Lead-free $K_{0.5}Na_{0.5}NbO_3$ (KNN) ceramics have revealed dielectric nature sintered between 1075 and 1150 °C showing the dielectric constant of 460 at 10 kHz [48]. Mg_2SiO_4 ceramic material sintered at 800 °C has displayed a dielectric constant of 14.13 revealing its significance for microwave communications [49]. Temperature-dependence of the dielectric nature of different materials strongly suggests the importance of the sintering process on the dielectric properties of the ceramic composite, BaO:ZnO, in the present study.

In the present article, BZO composite with BaO and ZnO in a 1:1 wt% ratio is prepared, via a simple autocombustion method, and investigated for the microstructural and dielectric properties after sintering from low 550 °C to intermediate temperature 950 °C. The outcomes suggest that the morphological changes and microstructural densification due to sintering affect the dielectric properties of the BZO ceramic composite.

1.1. Synthesis

All the starting chemicals (purity >99.0%) were purchased from Sigma-Aldrich. Zinc nitrate hexahydrate ($Zn(NO_3)_2·6H_2O$) and barium nitrate ($BaNO_3$) in the 1:1 wt% ratio was selected to synthesize the ZnO:BaO ceramic composite. A facile and cost-effective autocombustion method was adopted to prepare the composite material. Two solutions were prepared by dissolving zinc nitrate and barium nitrate in deionized water (DIW) in a 1:1 wt% ratio and heated at 90 °C for 15 min. After complete dissolution, both solutions were mixed and heated again at 90 °C for 15 min. Subsequently, after the thorough homogeneous mixing of the precursors'-solutions, oxalic acid was added and heated at 130 °C for 3 h until the completely dried powder was formed. During heating, oxalic acid in the solution acted as a fuel, eventually leading to the ultimate combustion reaction. Finally, after the calcined drying at 200 °C for 3 h, the powder was divided into five parts. All five amounts were sintered separately at 550, 650, 750, 850, and 950 °C for 2 h in the air. Cooling of all samples was done slowly to room temperature. The BaO:ZnO samples treated at 550 °C, 650 °C, 750 °C, 850 °C, and 950 °C were named BZO-1, BZO-2, BZO-3, BZO-4, and BZO-5 ceramic composites, respectively, throughout this article. A schematic of the synthesis

process is illustrated in Fig. 1.

The exothermic reactions involved in the synthesis were the following:

$$Ba(NO_3)_2 \xrightarrow{\text{Oxalic acid}} BaO\downarrow + 2NO_2\uparrow + \frac{1}{2}O_2\uparrow$$

$$Zn(NO_3)_2 \xrightarrow{\text{Oxalic acid}} ZnO\downarrow + 2NO_2\uparrow + \frac{1}{2}O_2\uparrow$$

$$BaO + ZnO + H_2O \xrightarrow{\text{Oxalic acid}} BaO:ZnO\downarrow + H_2O\uparrow$$

The byproducts later form nitric acid according to the following reaction, which was removed during the heating process.

$$4NO_2 + O_2 + 2H_2O \rightarrow 4HNO_3$$

1.2. Characterizations

X-ray diffraction was performed at D8 Advance, Bruker, with the X-rays source of CuK_α-1 of $\lambda = 1.54056$ nm.

Diffused reflectance UV–Vis spectroscopy of the prepared samples was done by PerkinElmer Lambda 950 setup.

Infrared Fourier Transforms spectra of the prepared materials in the range 4000–400 cm^{-1} were recorded by IRPrestige-21 by Shimadzu.

High-Resolution Raman System made by i-Raman® USA was considered for the inelastic measurements of the photon by the samples. The setup was operated at 50 mW at maximum, and a LASER of wavelength 532 nm was mounted with the Raman setup.

JEOLJSM-6480 LV scanning electron microscope (SEM) was considered to visualize the surface morphology of BaO:ZnO specimens fixed on carbon tape.

Agilent Cary Eclipse Fluorescence Spectrophotometer was used to record the emission peaks for 300–600 nm.

E4980A Precision LCR Meter by Agilent was used to record the dielectric properties of the prepared BZO ceramic composites. It was done in two modes: (i) Parallel capacitance and dissipation with the frequency of 20 Hz to 2 MHz and (ii) Parallel capacitance and resistance at the frequency of 20 Hz to 2 MHz. The accuracy was ±0.01%. The underlying approach in this setup was to record the capacitance by the parallel–equivalent circuit. Samples were pressed by 2500 MPa pressure for 5 min to create a disc-like shape with the same diameter of 13.78 mm ($A = \pi r^2$) and variable thicknesses (l) of 1.39 mm of BZO-1, 0.23 mm of BZO-2, 1.30 mm of BZO-3, 1.04 mm of BZO-4, and 1.44 mm of BZO-5. Dielectric constant ε' [50] was estimated by

$$\varepsilon' = \frac{C \times l}{A \times \varepsilon_o}$$

where $\varepsilon_o = 8.854 \times 10^{-12}$ Fm^{-1} correspond to the permittivity of free space.

Due to the availability of a low amount of BZO-2 sample, the thickness was as minimum as 0.23 mm and was less than the other four samples. Further, only for the BZO-2, this led to producing noise in the various dielectric measurements at a low frequency. This can be seen in the various quantities obtained during dielectric measurements where the original data of the BZO-2 composite is plotted.

2. Results and discussion

2.1. XRD results

The peaks at 23.73°, 24.19°, 27.6°, 30.0°, 33.87°, 40.33°, 41.77°, 44.70°, and 46.57° correspond to (201), (211), (102), (310), (212), (111), (200), (112), and (103), respectively, and matched with the JCPDS card no. 26–0178 [51] as a tetragonal structure of BaO. The peaks at 31.64°, 34.28°, 36.1°, 47.4°, 56.38°, 62.6°, and 68.43° correspond to (100), (002), (101), (102), (110), (103), and (112), respectively, matched well with the JCPDS card no. 31–1451 with the hexagonal structure of ZnO [52]. The diffraction patterns of all five samples are shown in Fig. 2. In Fig. 3, it is depicted that after a moderate temperature (550–950 °C) heat treatment, there is no phase transformation observed.

Lattice parameters of BaO and ZnO structures are calculated for selected diffraction peaks as listed in Table 1. Lattice parameters, interplanar spacing and crystallite size all vary with temperature. In contrast to the continuous change in the crystallite size, which is purely a temperature effect, the lattice constants are not changing monotonically.

Asymmetric X-ray diffraction (XRD) peak shifting with temperature, shown in Fig. 4, indicates that the BaO (201) peak shifts to the lower angles till 850 °C and then moves to the higher angle at 950 °C. In the case of ZnO, a similar irregular trend is seen for the (101) peak shifting. Such behavior is present in all the diffraction peaks throughout all the measured diffraction patterns. This is well-known from the literature on composite materials that the different phases coexist with different coefficients of thermal expansion and metal oxidation states behave differently during sintering [53]. The shifting of X-ray diffraction peaks to the lower angles is not large because the diffraction patterns of ceramic composites, BZO-1 to BZO-5, are recorded at room temperature after the heating in the 550–950 °C range for equal durations. Since

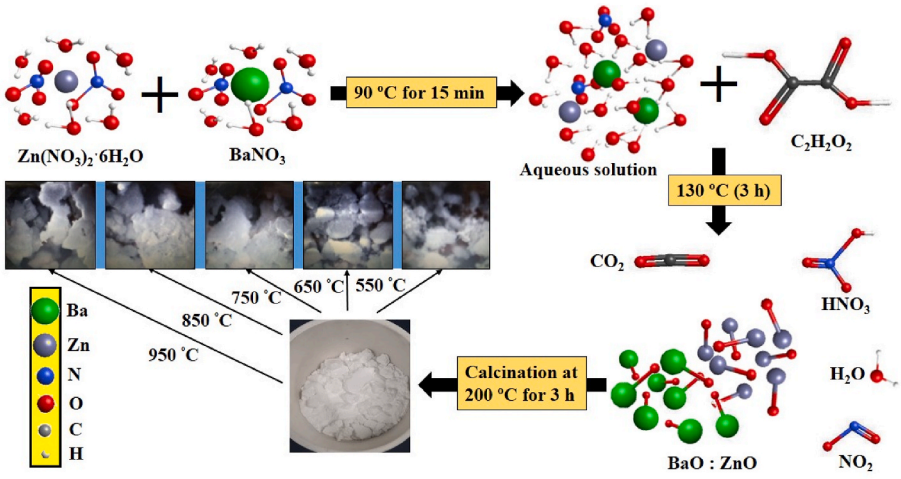

Fig. 1. Schematic of the synthesis procedure.

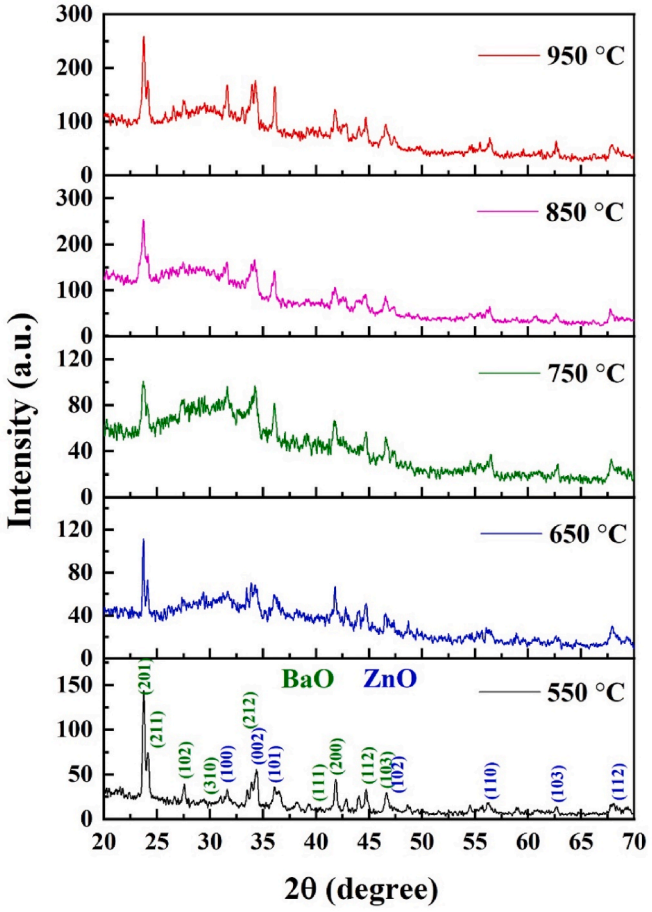

Fig. 2. X-ray diffraction profiles of BaO:ZnO composite material sintered at different temperatures. The diffraction pattern obtained after sintering at 550 °C is indexed with the hkl-planes of BaO and ZnO phases.

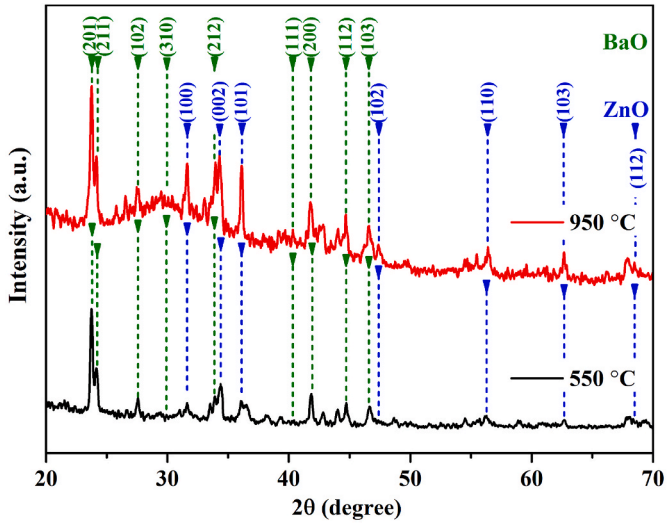

Fig. 3. Comparison of X-ray diffraction profiles of BaO:ZnO composite material sintered at 550 °C and 950 °C.

there is no doping in the BaO and ZnO phases of ceramic composites, therefore, the minute variation in the X-ray diffraction peaks is attributed to the internal stresses, defects, inter-crystallite boundary mismatch and crystallite size. Moreover, the lattice expansion of BaO or ZnO is associated with the energy that arises from the inter-crystallite mismatch. The mismatch will affect less to the lattice parameters and influence more to the crystallite size of both BaO and ZnO (Table 1) which can be critical to the polarization phenomenon. The shifting of the peaks is very small till 850 °C and at a maximum temperature of 950 °C, they slide to the higher angles showing the BZO-5 ceramic composite under relaxation. In other words, the defects are healed at higher temperatures.

Data presented in Table 1 is plotted further to investigate the effect of sintering temperature on the normalized lattice parameters. The random variation of lattice parameters a and c of BaO are given in Fig. 5a. This indicates inconsistent variations of lattice parameters in all the ceramic samples after heating at different temperatures. The differentials are small along a-side (0.18%) and large in the case of the c-side (0.30%) of the BaO unit cell. This shows more strain along the c-side of the BaO lattice. For ZnO, symmetric variations along the a- and c-sides are noticed at all sintering temperatures except 850 °C, for which the c-value drops, as shown in Fig. 5b. Overall, the variations in a-side and c-side are 0.06% and 0.21%, respectively. This is well-known that the addition of an element in a crystalline matrix leads to variation in the lattice structure [54]. But in the present case, BaO and ZnO have common interfacial boundaries without any doping. The lattice mismatch gives rise to the strain on and in the vicinity of BaO and ZnO inter-crystallite boundaries. In the current ceramic composite, the increase in activation energy is proportional to the increasing temperature, where temperature plays its role in reducing the crystallite boundary tension not only between the BaO and ZnO phases but also easing the inter-crystallite strain in the same phase. Eventually, the lattice parameters were also affected.

2.2. Raman analysis

Raman spectra of BaO:ZnO ceramic composite sintered at 550 °C and 950 °C are shown in Fig. 6. Regarding BaO, characteristic Raman peaks are present at 132 and 213 cm^{-1} [55]. Similarly, in small intensity, the ZnO Raman modes also exist at 149, 331 382, 433, and 581 cm^{-1} and are attributed to the fundamental phonon scattering [56,57]. In the Raman spectrum recorded after sintering at 950 °C, BaO and ZnO peaks remain the same confirming that there is no phase transition. For ZnO, the peak at 149 cm^{-1} after sintering at 950 °C shows its growth. Further, the prominency of this peak, after sintering at 950 °C, is due to the decrease in the defects in the ZnO phase. Since Raman spectroscopy is sensitive to molecular structures, therefore, Ba–O and Zn–O, as a molecular framework, exhibit distortion upon LASER interaction during Raman measurement. In the case of the Zn–O bond, the improved peak at 149 cm^{-1} shows that it is easy to relocate as compared to the Ba–O bond. In other words, polarization is easily produced in the Zn–O phase. This is also connected with the present dielectric investigations of the BZO ceramic composite.

2.3. UV–Vis DRS analysis

The diffused reflectance spectra, in terms of reflectance versus wavelength, of all sintered ceramic samples are shown in Fig. 7a. The corresponding band gap energies are indicated in Fig. 7b. The band gap energy (E_g) of BaO is determined as 3.61, 3.6, 3.59, 3.55, and 3.52 eV after sintering at 550, 650, 750, 850, and 950 °C, respectively. Similarly, the E_g of ZnO is obtained as 3.24, 3.23, 3.21, 3.20, and 3.19 eV after sintering at 550, 650, 750, 850, and 950 °C, respectively. The crystallite size (D) and E_g for BaO:ZnO ceramic composites are plotted in Fig. 8a,b. The sintering of material increases crystallite size but decreases in the E_g for both BaO and ZnO phases.

2.4. Photoluminescent measurements

Photoluminescent (PL) spectra of sintered composites are shown in Fig. 9 for the 272.03 and 391.96 nm excitation wavelengths. PL emission peaks of BaO after sintering at 550, 650, 750, 850, and 950 °C are

Table 1
Structural detail of ceramic composite BaO: ZnO. Lattice parameters of BaO are calculated by considering (200) and (111). For ZnO, the lattice parameters are computed by (100) and (002). For interplanar spacing and crystallite size calculations of BaO and ZnO, the (201) and (101) peaks have been considered, respectively.

Sample	Temp. (°C)	BaO				ZnO				
		a (nm)	c (nm)	$d_{(201)}$ (nm)	$D_{(201)}$ (nm)	a (nm)	c (nm)	c/a	$d_{(101)}$ (nm)	$D_{(101)}$ (nm)
BZO-1	550	0.4312	0.3269	0.3743	41.36	0.3267	0.5237	1.603	0.24893	22.23
BZO-2	650	0.4318	0.3253	0.3748	59.21	0.3264	0.5218	1.597	0.24907	24.75
BZO-3	750	0.4328	0.3257	0.3752	76.37	0.3275	0.5247	1.602	0.2490	27.74
BZO-4	850	0.4322	0.3240	0.3748	83.77	0.3268	0.5255	1.609	0.24887	36.77
BZO-5	950	0.4320	0.3279	0.3744	92.54	0.3274	0.5240	1.600	0.24853	40.99

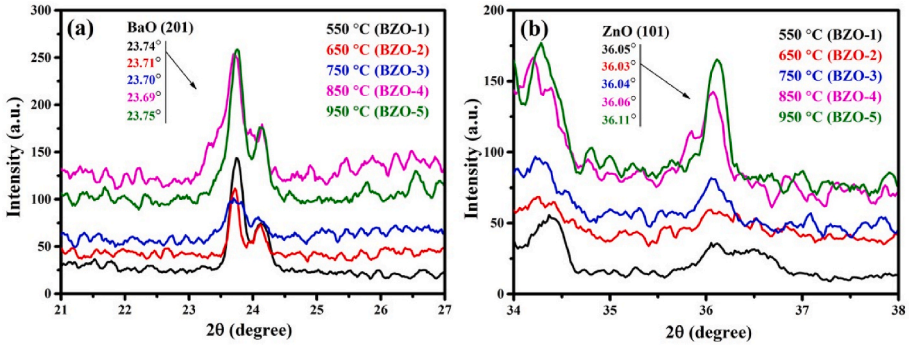

Fig. 4. XRD peak shifting of BaO and ZnO as a function of sintering temperature.

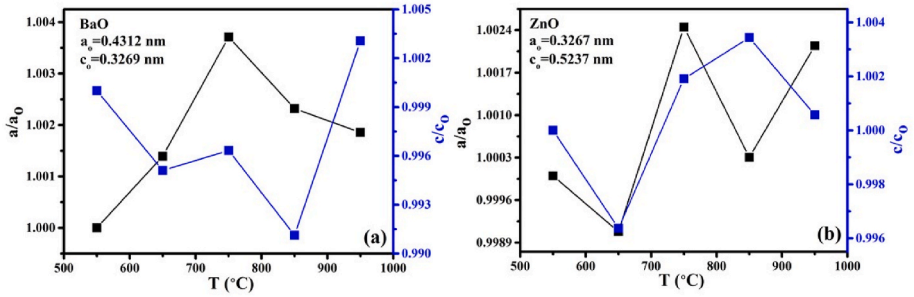

Fig. 5. Normalized cell parameters of BaO and ZnO phases Vs sintering temperature.

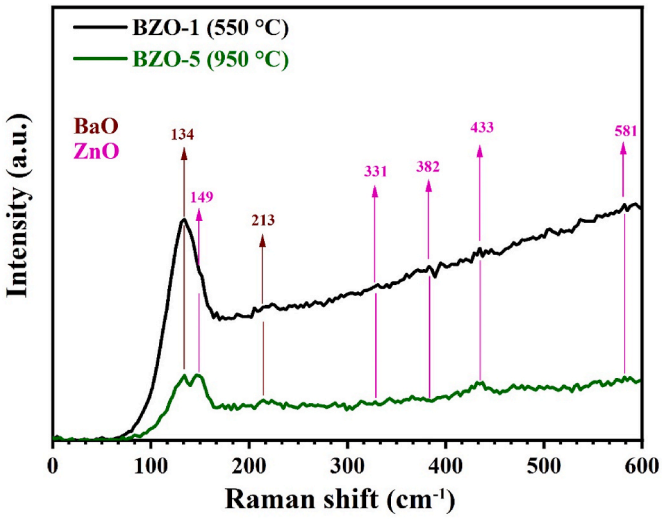

Fig. 6. Comparison of Raman spectra of BZO-1 and BZO-5 composites sintered at 550 °C and 950 °C.

measured as 534, 500, 478, 469, and 434 nm, respectively. For ZnO, the PL emission is 411, 388, 366, 345, and 321 nm noted for the composites sintered at 550, 650, 750, 850, and 950 °C, respectively. There is a shifting of the PL peak towards the lower wavelength with increasing sintering temperature for both BaO and ZnO phases [58]. An increase in the sintering temperature leads the annealing process to take place and inner structural defects of BaO and ZnO start recovering. At low temperatures, due to the small particle size of BaO and ZnO, the surface oxygen vacancies (defects) bind the freely moving electrons among the particles to form sub-bands. Hence the excitation process is strong at lower temperatures [59]. With an increase in temperature, particle size increases causing the recombination process gets weaker affecting the excitation process.

2.5. FTIR analysis

Fourier Transform IR spectra of sintered composite specimens are shown in Fig. 10a. A peak at 619 cm^{-1} is due to Ba–O stretching vibrations. Similarly, a strong Ba–O bond is indicated at 693 cm^{-1}. The O–H stretching mode is present at 1750 cm^{-1} [52]. A peak at 1057 cm^{-1} is attributed to the stretching vibration of O–O bond [60]. Two peaks at 858 and 2453 cm^{-1} are connected to the asymmetric vibrational modes of NO_3^{-1} ions and $-CO_2$ bond, respectively [61]. A metal-oxygen bond observed at 505 cm^{-1} is a characteristic mode of Zn–O [62]. Another

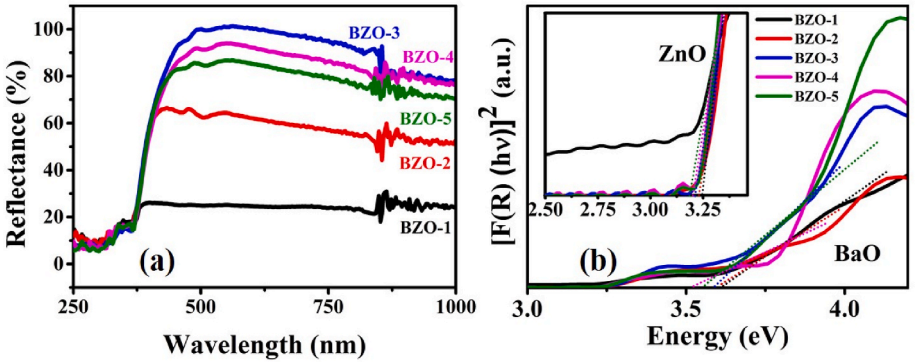

Fig. 7. (a) UV-DRS spectra of BaO:ZnO ceramic composite. (b) Band gap energies of BaO:ZnO composites, BZO-1, BZO-2, BZO-3, BZO-4, and BZO-5, sintered at 550, 650, 750, 850, and 950 °C.

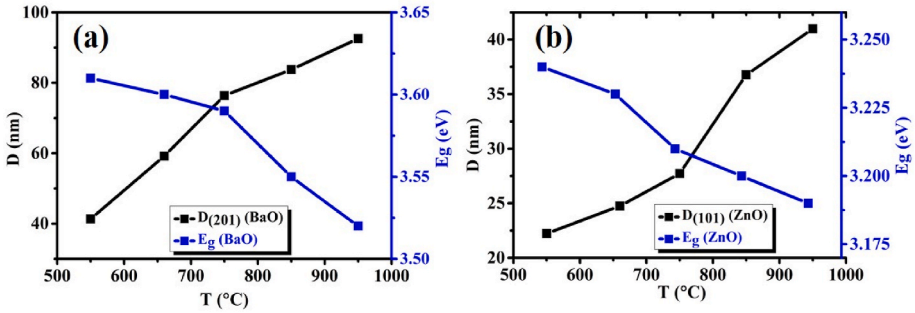

Fig. 8. (a) Effect of sintering temperature on the crystallite size (D) and band gap energies (E_g) of BaO (a) and ZnO (b) in composite form.

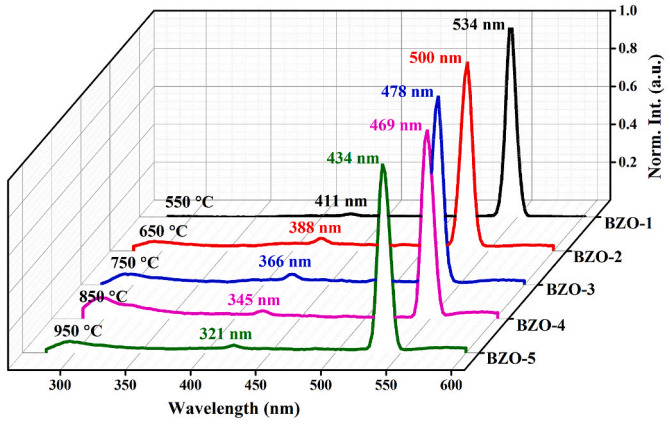

Fig. 9. Effect of sintering temperature on the excitation peaks of BaO and ZnO.

stretching mode of vibration seen at 422 cm^{-1} is the signature of the ZnO nanoparticles [63]. A peak at 1413 cm^{-1} corresponds to the asymmetrical and symmetrical stretching modes of carboxylate groups [64]. Peaks at 1349, 816, and 729 cm^{-1} correspond to the $Ba(OH)_2$ [65] that persist until 650 °C during the sintering. These transmittance peaks of $Ba(OH)_2$ disintegrate on further heating and are therefore absent in the FTIR spectra measured at 750, 850 and 950 °C. The effect of the $Ba(OH)_2$ phase in the measurements of the dielectric constant has been noticed and explained in the relevant section.

2.6. SEM analysis

Scanning electron micrographs of all the sintered samples are shown in Figs. 11–13. There are growing morphological changes in the material according to the increase in the sintering temperatures from 550 to 950 °C. There are clusters of cloudy particles of approximately 100 nm in both BaO and ZnO in the case of BZO-1 (Fig. 11). Both metal oxides together develop a porous network of BaO and ZnO particles interface to each other. Even the ZnO is denser as compared to the BaO.

After sintering at 650 °C and 750 °C, the scanning electron micrographs of BZO-2 and BZO-3, respectively, are shown in Fig. 12a–d. The densification effect in the particles is observable along with the size-growth of particles, as in Fig. 12a and b. BaO becomes more compact than the BZO-1 (Fig. 11) and the smaller particles coarsened into the large ones. After sintering at 750 °C, overlapped ZnO rectangular surfaces are developed, as shown in Fig. 12c and d. The aggregates of BaO are settled on and in between the rectangular ZnO surfaces. There are also ZnO-stacked surfaces in the form of plateaus, as indicated in Fig. 12d.

Scanning electron micrographs of BZO-4 and BZO-5 sintered at 850 °C and 950 °C, respectively, are shown in Fig. 13a–d. Growing particles developed surface over-surface structure and seemed like flowers when viewed at the 5 m scale (Fig. 13a,c). These flower-like structures correspond to the ZnO material. These flowers are based on stacked ZnO surfaces, whereas the BaO becomes dense but less than the ZnO. After sintering at 950 °C, the particles' surface roughness is reduced as seen in the better contrast of the neighboring particles presented in the SEM image in Fig. 13d. Further, this is associated with the increasing size of the particles.

Metal oxides are tough and do not disintegrate at intermediate temperatures. BaO and ZnO show mechanical stability due to the high chemical reactivity attributed to the change requiring a higher temperature. In the prepared composites, both the metal oxides, sintered at increasing temperatures, the respective particles are motivated kinetically to get diffused into each to form large size agglomerated appearance, as seen in Figs. 11–13, for all five samples. Intergrain alignment of crystallographic planes leads to develop the orientational distribution to make BaO or ZnO smaller particles get in contact. In this process, there is also a possibility of interparticle surface diffusion of atoms at different

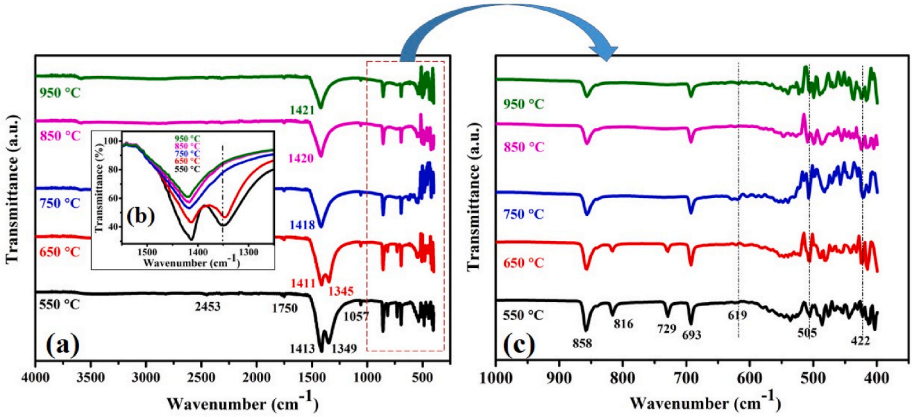

Fig. 10. (a) FTIR spectra of BZO-1, BZO-2, BZO-3, BZO-4, and BZO-5 already sintered at 550, 650, 750, 850, and 950 °C, respectively. (b) $Ba(OH)_2$ disintegration during sintering between 750 and 850 °C. (c) FTIR spectra for small k-range.

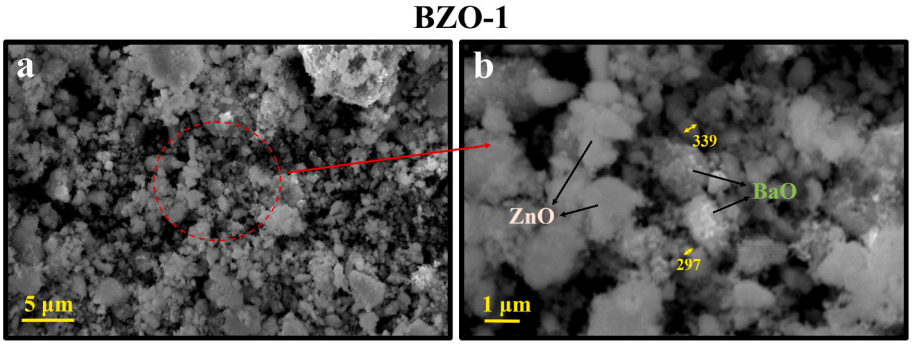

Fig. 11. SEM images of BZO-1 (sintered at 550 °C). All the marked sizes of the particles are in nm.

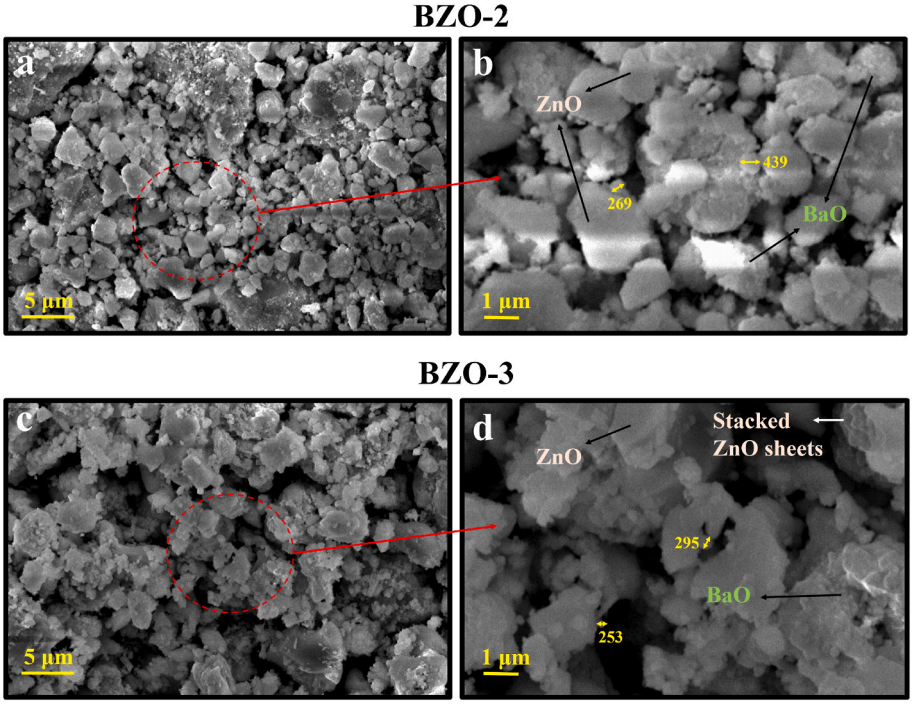

Fig. 12. SEM images of BZO-2, sintered at 650 °C (a,b) and BZO-3 sintered at 750 °C (c,d). All the marked sizes of the particles are in nm.

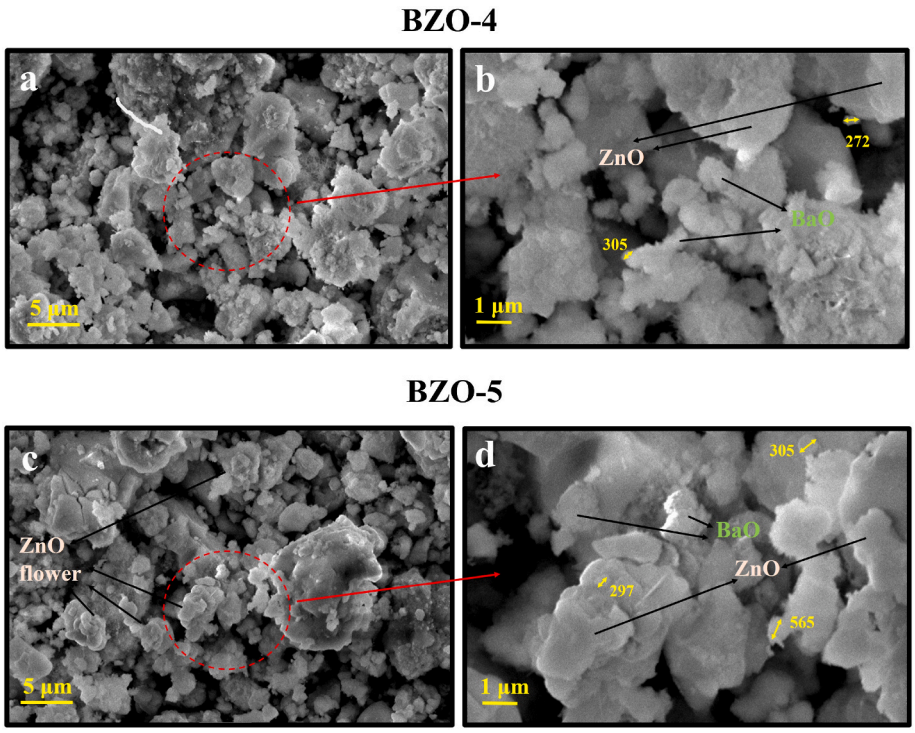

Fig. 13. SEM images of BZO-4 sintered at 850 °C (a,b) and BZO-5 sintered at 950 °C (c,d). All the marked sizes of the particles are in nm.

rates due to size and shape differences. This mechanism leads to particle growth in BaO and ZnO materials during sintering from 550 °C to 950 °C and is evident from the SEM analysis.

On heating, the respective BaO or ZnO phases have more probability to increase their crystallite size by overcoming the inter-crystallite (boundary) tensions of the same phase instead of diffusion of BaO and ZnO into each other. Thus particle agglomeration is seen in their respective phases as observed in the X-ray diffraction analysis (Fig. 8). Further, instead of particle size, the crystallite size and inter- and intra-crystallite boundary are more crucial for the dielectric properties of the BaO:ZnO ceramic composite. With the increase in temperature, the increase in the crystallite size reduces inter- and intra-crystallite boundaries leading to a decrease in the interfacial polarization. Thus the morphological changes in the BaO:ZnO ceramic composite as a function of temperature can affect the dielectric constant.

2.7. Dielectric properties

The capacitance and dielectric constant with respect to the input signal in the frequency range are shown in Fig. 14a and b. Decrease in the capacitance is observed with sintering temperature. While the dielectric constant first decrease between 550 and 650 °C and then it increases to 950 °C. The possible reason behind the decrease in the dielectric constant, while heating from 550 to 650 °C, is the existence of the residual $Ba(OH)_2$ phase remaining there from synthesis. After heating more than 650 °C, $Ba(OH)_2$ is no more present [65] as confirmed in the FTIR analysis (ref. Fig. 10a and b). The capacitance and dielectric constant at higher frequency regions remain uniform, revealing their potential for communication applications in the high-frequency regime [35]. For the 0.5–2.0 MHz, C_p-variation is small and is in the order of 0.03 in the case of BZO composites sintered at 750, 850 and 950 °C, indicated in the inset Fig. 14 a1. The dielectric constant ε′ varies by 0.5 among the BZO composites sintered more than the 550 °C in the 0.0–2.0 MHz (Fig. 14 b1). The dielectric constant ε′ of BZO-1 sintered at 550 °C, continues to decrease in the same frequency limit.

The impedance of the sintered composite is given in Fig. 15a. By increasing the sintering temperature, the impedance increases between 0.0 and 1.0 MHz range (Fig. 15 b1), whereas at higher frequencies, they

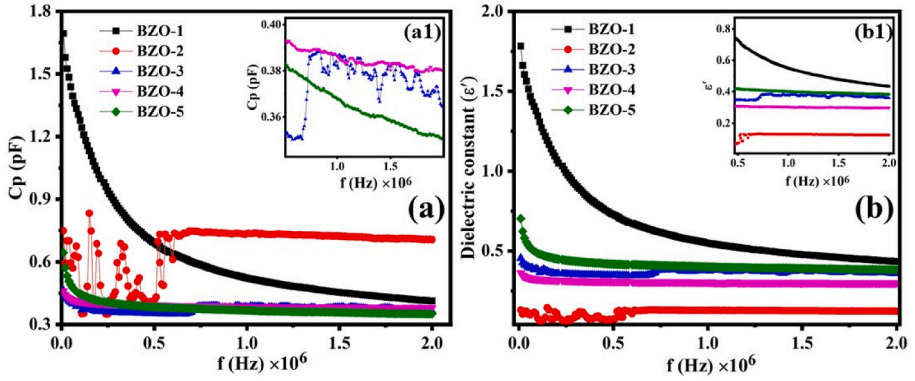

Fig. 14. (a) Parallel capacitance (C_p) with respect to frequency of BaO:ZnO composites sintered at 550 °C, 650 °C, 750 °C, 850 °C, and 950 °C. (b) Changes in the dielectric constant (ε′) with the frequency of BaO:ZnO composite sintered at different temperatures.

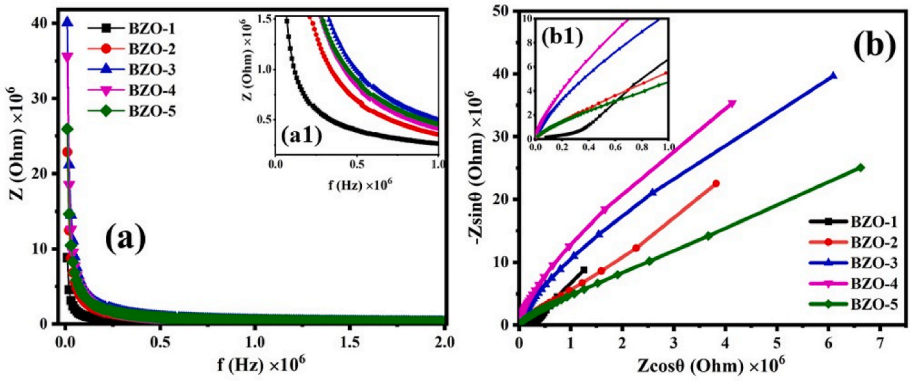

Fig. 15. (a) Impedance versus frequency for BaO:ZnO composites sintered at 550 °C (BZO-1), 650 °C (BZO-2), 750 °C (BZO-3), 850 °C (BZO-4), and 950 °C (BZO-5). (b) Nyquist plot of the complex impedance of BaO:ZnO composites sintered at different temperatures.

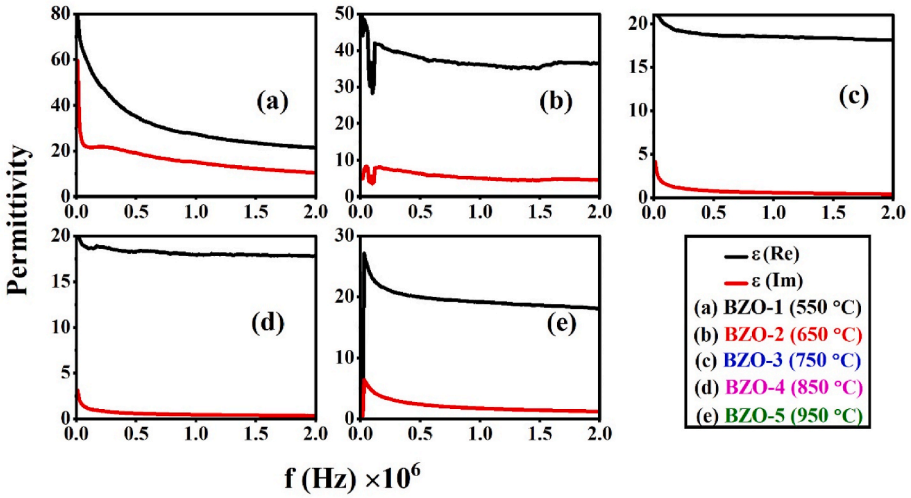

Fig. 16. Variation of ε(Re) and imaginary ε(Im) parts of permittivity (in F/m) with the frequency of BaO:ZnO composites sintered at different temperatures.

converge. Nyquist plot between the real and imaginary parts of the impedance is shown in Fig. 15b for the sintered ceramic composites. Non-uniform trends among the composites are noted.

The real ε(Re) and imaginary ε(Im) permittivity of all the ceramic composites are shown in Fig. 16. Both the components exhibit decrease over the temperature range of 550–950 °C. Overall ε(Re) reduces by 7 F/m and ε(Im) by 8 F/m at 2.0 MHz. Large values of ε(Re) and ε(Im) may be due to the perpetuated polarization paths [66] developed among the BaO and ZnO crystallites during the sintering at different temperatures. Moreover, ε(Re) and ε(Im) remain constant in all the BZO composites after 0.5 MHz except for the BZO sintered at 550 °C.

The effect of heat treatment on the conductivity of the prepared

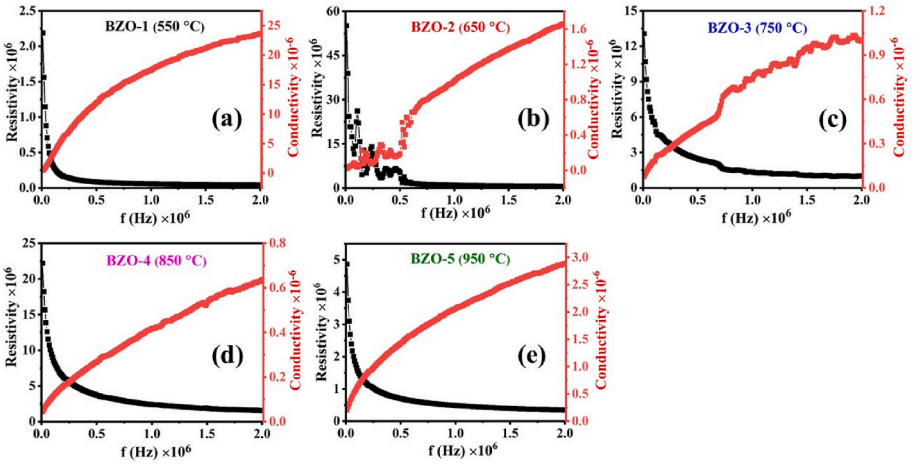

Fig. 17. Variation of conductivity ($S \cdot m^{-1}$) and resistivity ($Ohm \cdot m^{-1}$) BaO:ZnO composites sintered at different temperatures.

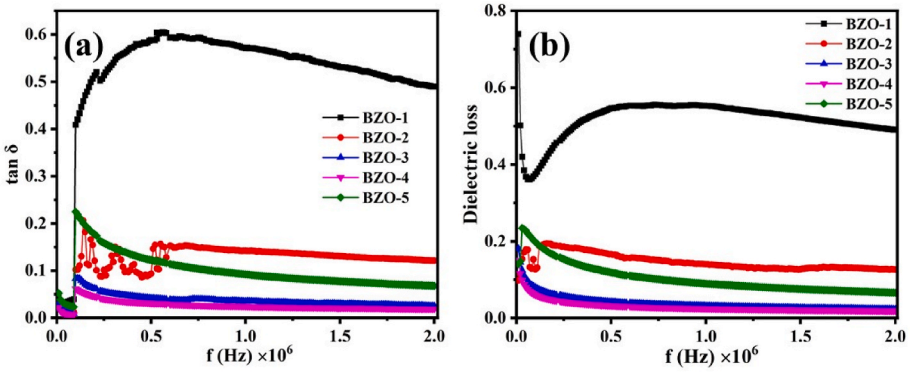

Fig. 18. Effect of sintering temperatures on the dielectric loss (tangent loss) of BaO:ZnO composites.

composites is shown in Fig. 17a–e. It decreases continuously for the composites sintered at different temperatures except for the BZO-5, which shows a slight increase but is still less than the BZO-1 sintered at 550 °C.

Fig. 18a presents the dependence of the loss tangent (tanδ) as a measure of loss of applied signal with the frequencies of applied signal for all the BZO ceramic composites. Large tanδ among the prepared composites is exhibited by BZO-1, while it decreases twice for the other BZO composites. Interestingly, in the case of BZO-1 sintered at 550 °C, tanδ increases to 0.6 MHz and then starts showing a continuous reduction up to 2.0 MHz. On the other hand, such behavior is absent in all other composites. This is due to the densification of the structure that takes place during sintering and finally affects the polarization phenomenon. In other words, more uninterrupted channels of polarization become available after heat treatment [67]. Therefore, heat-treated BZO composites show less energy dissipation (Fig. 18b). Composites sintered above 550 °C reveal less energy loss of the applied signal than the others.

For different alternating input signals of 0.5, 1.0, 1.5, and 2.0 MHz, the ε(Re), ε(Im), ε′ and tanδ are plotted in Fig. 19a–d. In all the cases, there is a decreasing trend at large frequencies. Also, this gives information on the dielectric properties of BaO:ZnO ceramic composite with the temperatures.

This is well-known that particle shape and size distribution, crystal type, crystallinity, and porous volume among the particles define certain physical, chemical, or other properties from the applications point of view. In the present case, the compactness of the morphological structure of BaO:ZnO ceramic composite as a result of heating is responsible for the change of dielectric response [68]. Structural faults, both in BaO and ZnO that healed during the sintering is proposed reason for the dielectric loss reduction. As ceramic, the sintered BaO:ZnO composites, the suggested nature of polarization is interfacial at low frequencies that prevail through displacement and ionic polarization mechanisms [69]. The different relaxation times of different ions at varying frequencies [70] can also affect the response of BZO composites with increasing crystallite sizes. Except, for the dielectric constant (Fig. 19c) most of the parameters (Fig. 19a,b,d) reduce in a non-linear fashion in the 0.5–2.0 MHz range.

Inside the BZO composite, the polarization along the boundaries

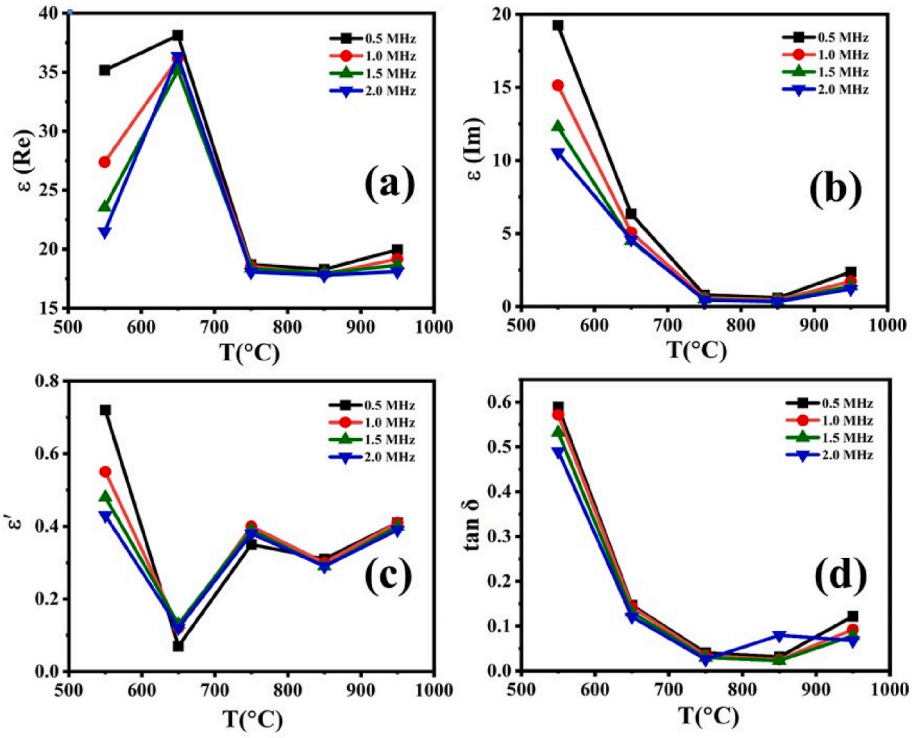

Fig. 19. At different frequencies, the effect of sintering temperature on the real part of permittivity ε(Re) (a), the imaginary part of permittivity ε(Im) (b), dielectric constant ε′ (c), and loss tangent (d).

between the BaO and ZnO crystallites is significant for the net dielectric response. On sintering, the total length of all crystallite boundaries of BaO and ZnO inside a composite particle reduces, allowing to decrease in the polarization mismatch accross the boundaries. Moreover, the orientational differences based on crystalline natures present in the vicinity of the interfacial boundaries can affect the polarization in a nonuniform manner. Since locally the variations in the crystallite boundaries with sintering temperature are not fully controlled; therefore, the polarization variation is not perfectly consistent with the increasing temperatures. Eventually, the crystallite boundaries variation as a function of sintering temperature deliver uneven dielectric behavior of composites when analyzed in the 0.0–2.0 MHz range. According to the literature, the magnetic, electric, dielectric and electronic properties of materials can be changed via grain size variations through sintering or annealing [71,72]. In the present case, the decrease in the dielectric constant of the BZO ceramic composite (Fig. 19c) is attributed to the existence of residual $Ba(OH)_2$ phase till 550–650 °C. For the later heating in the 750–950 °C range there is a gradual increase in the dielectric constant. In Fig. 20, the dielectric constant is plotted against the crystallite size of the BaO and ZnO, where a decrease in the dielectric constant can be seen with the increase in the crystallite size for BZO-2. Afterward, there is an increasing dielectric constant of BZO-3, BZO-4, and BZO-5 at all frequencies due to sintering.

The polarization process that takes place inside the BZO ceramic composite is based on interfacial polarization and ionic polarization (dipole polarization). When BZO ceramic composite is exposed to the electric field signal, ZnO polarizes easily compared to the BaO due to the difference in Ba and Zn charge concentrations. Thus ionic polarization in ZnO is more as compared to BaO. Hence large ionic polarization contribution is provided by ZnO at all temperatures. Thermal point of view, BaO has a slightly large heat capacity as compared to ZnO. Therefore, due to the increase in temperature, the increase in crystallite size is slightly more in the case of ZnO as compared to BaO (SEM analysis). On the other hand, the polarization strength over the crystallite boundary (red line in Fig. 21), called interfacial polarization, decreases due to an increase in crystallite size. Moreover, the misalignment of the dipole vectors of BaO and ZnO dipoles over the crystallite boundaries also decreases with increasing sintering temperature. Further, this is suggested that the interfacial crystallographic orientational mismatch over the BaO and ZnO crystallite boundaries also plays a role in the interfacial polarization. During sintering interfacial length of boundaries increase and interfacial crystallographic orientational mismatch decreases.

Interfacial mismatch and interfacial polarization are coupled with each other. Ionic (dipole) polarization and interfacial polarization are illustrated in Fig. 21. There are three types of crystallite boundaries involved in the polazarization phenomenon of BaO:ZnO ceramic composite as a dielectric. 1) Intra-crystallite boundary between the crystallites of BaO or ZnO, 2) Inter-crystallite boundary between the two same grains of BaO or ZnO and 3) Interfacial boundary between the BaO and ZnO grains as illustrated in Fig. 22.

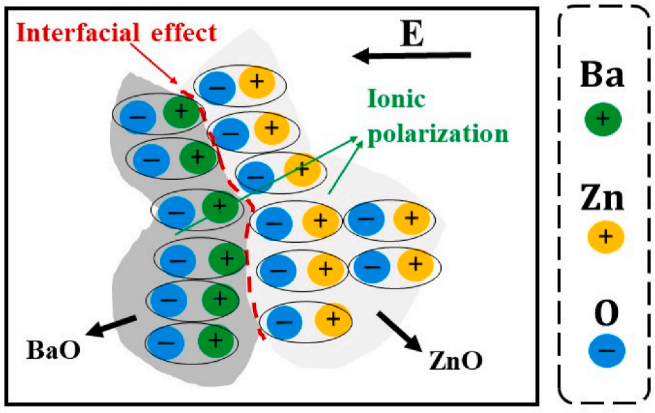

Fig. 21. Illustration of the interfacial polarization and ionic polarization between BaO and ZnO crystallites in the BZO composite.

As a result of sintering process the crystallite size increases, crystallite boundaries reduce. This leads to reducing the interfacial crystallographic orientational mismatch and also decreasing the interfacial polarization between BaO and ZnO. At low temperatures crystallite boundary distribution within BaO and ZnO is large and the probability of the interfacial crystallographic orientational mismatch is high. This suggests reduced polarization at low sintering temperatures. But in the present case, the dielectric constant for composites sintered at 550–650 °C is not fully associated with the BaO:ZnO but also there is a contribution of unwanted $Ba(OH)_2$ phase left from the synthesis procedure. On the other hand, at higher temperatures >650 °C, the residual $Ba(OH)_2$ phase is disintegrated. Also at higher temperatures, due to the large size of crystallites, less amount of crystallite boundaries, in BZO composite, are available for interfacial crystallographic orientational mismatch and interfacial polarization. As a result, the ionic polarization of the composite sintered above 650 °C is getting significant as compared to the interfacial one due to the large crystallite size. Moreover, the polarization mechanisms for the low and high-frequency regimes are the same in the case of BaO:ZnO composite as demonstrated in detail in Fig. 22.

In summary, the stability of dielectric constant ε′, permittivities ε(Re), and ε(Im) of the prepared BZO ceramic composite can be seen in the 0.25–2.0 MHz range except for the BZO-1 sintered at 550 °C. In the case of BZO-1, a continuous decrease is noticed. Similar behavior is present for the loss tangent (tanδ). This suggests controlling the dielectric behavior by simply the sintering process and tuning the material for desired frequency range.

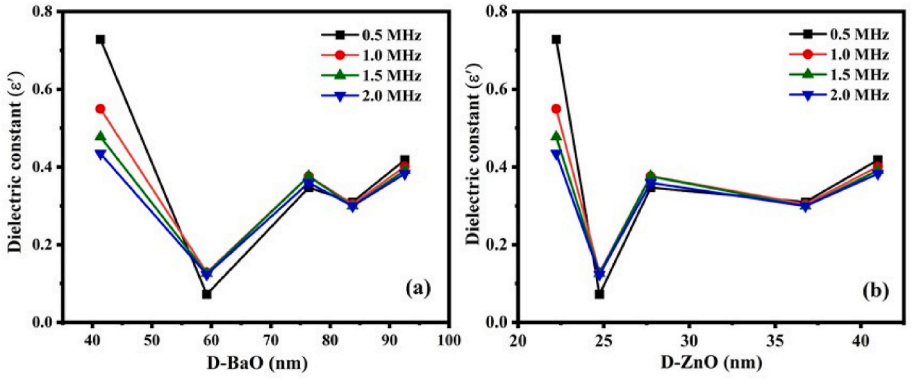

Fig. 20. At different frequencies, the effect of crystallite size (as a function of sintering temperature) on the dielectric constant ε′.

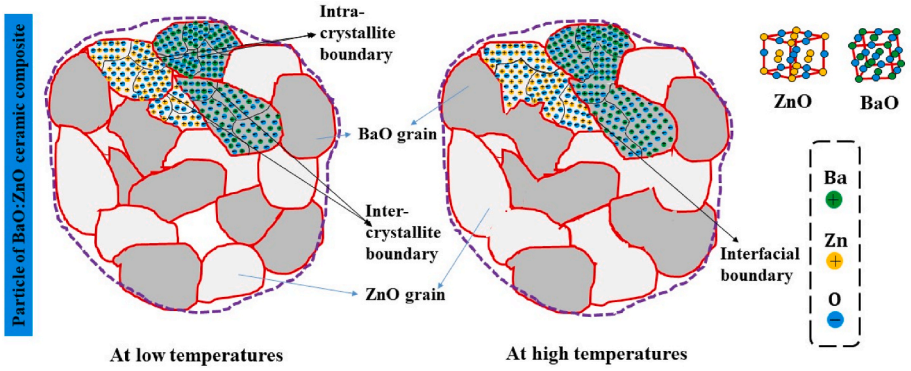

Fig. 22. Model sketch of polarization of BaO:ZnO ceramic composite, as a dielectric, demonstrating the role of interfacial mismatch, inter- and intera-crystallite boundary variation as a consequence of heat treatment.

3. Conclusion

One pot easy, quick and economical autocombustion method has been implemented to synthesize the BaO:ZnO (BZO) ceramic composite. Sintering of the BZO composite between 550 and 950 °C led to the development of the crystalline structure with increasing BaO and ZnO crystallite size. Morphological variations by sintering in terms of an increase in the particle size, change of particle shape, and increase of smoothness of particles have been noticed as the microstructural formation of BZO composite. Band gap energies of both BaO and ZnO vary as a function of increased crystallite size. Along with the microstructural investigations, the dielectric analysis of BZO composites sintered between 550 and 950 °C revealed that after a decrease in the dielectric constant till 650 °C, an increasing behavior has been observed for 750–950 °C in the frequency range of 0.0–2.0 MHz. Similarly, the permittivity, conductivity, and loss tangent have also exhibited a uniform trend in the signal range of 0.0–2.0 MHz. The dielectric constant ε' changes from 1.8 to 0.14 at a minimum frequency and 0.44 to 0.12 at a maximum frequency as the effect of sintering. The dielectric constants for BZO ceramic composites with different values remained stable between 0.25 and 2.0 MHz signals except for one sintered at 550 °C. This suggests that the dielectric constant of a material can be tuned in a desired frequency range simply by the sintering process. Therefore, the current BZO composite appeared as a ceramic material with a low dielectric constant stable over 0.0–2.0 MHz and can be another candidate for fast signal communication purposes in the high-frequency regime.

Credit author statement

MH-Muhammad Haseeb, MI-Muneeb Irshad, MS-Mohsin Saleem, AA-Abid Aleem, MA-Muhammad Arshad, AS-Atif Shahbaz, MI-Muhammad Imran, RG-Rabia Ghaffar, HAI-Hafiz Ahmad Ishfaq, AG-Abdul Ghaffar, Conceptualization, AG, MS, MI; Methodology, MH, AG; Measurements, MA, MS, MI; Formal analysis, MH, AG; Writing—original draft preparation, MH; Review and editing, AG, MS, MI; English language editing & discussion, RG; Discussion. AG, MH, MI, MS, AA, AS, MI, HAI; Supervision, AG. All authors have read and agreed to the published version of the manuscript. The list of authors is final.

Declaration of competing interest

The authors declare that they have no known competing financial interests or personal relationships that could have appeared to influence the work reported in this paper.

Acknowledgment

Not considered.

References

[1] H.P.P.V. Shanmugasundram, E. Jayamani, K.H. Soon, A comprehensive review on dielectric composites: classification of dielectric composites, Renew. Sustain. Energy Rev. 157 (2022), 112075, https://doi.org/10.1016/j.rser.2022.112075.
[2] X. Bi, L. Yang, Z. Wang, Y. Zhan, S. Wang, C. Zhang, Y. Li, Y. Miao, J. Zha, Construction of a three-dimensional $BaTiO_3$ network for enhanced permittivity and energy storage of PVDF composites, Materials 14 (2021) 3585, https://doi.org/10.3390/ma14133585.
[3] M. Saleem, I.S. Kim, J.S. Song, S.J. Jeong, M.S. Kim, S. Yoon, Synthesis, sintering and dielectric properties of a $BaTiO_3$–Ni composite, Ceram. Int. 40 (5) (2014) 7329–7335, https://doi.org/10.1016/j.ceramint.2013.12.075.
[4] H. Wu, F. Zhuo, H. Qiao, L.K. Venkataraman, M. Zheng, S. Wang, H. Huang, B. Li, X. Mao, Q. Zhang, Polymer-/Ceramic-based dielectric composites for energy storage and conversion, energy environ, Materials 5 (2021) 486–514, https://doi.org/10.1002/eem2.12237.
[5] R. Ma, B. Cui, D. Hu, S.M. El-Bahy, Y. Wang, I.H. El-Azab, A.Y. Elnaggar, H. Gu, G. A.M. Mersal, M. Huang, V. Murugadoss, Enhanced energy storage of lead-free mixed oxide core double-shell barium strontium zirconate titanate@magnesium aluminate@zinc oxide-boron trioxide-silica ceramic nanocomposites, Adv. Compos. Hybrid Mater. 5 (2022) 1477–1489, https://doi.org/10.1007/s42114-022-00509-z.
[6] J. Wang, H. Wu, Z. Wang, W. He, C. Shan, S. Fu, Y. Du, H. Liu, C. Hu, An ultrafast self-polarization effect in barium titanate filled poly(vinylidene fluoride) composite film enabled by self-charge excitation triboelectric nanogenerator, Adv. Funct. Mater. 32 (2022), 2204322, https://doi.org/10.1002/adfm.202204322.
[7] A. Aleem, A. Ghaffar, N.M. Kiani, M. Irshad, I. Mehmood, M. Shahzad, A. Shahbaz, Broad-band dielectric properties of teflon, bakelite, and air: simulation and experimental study, Mater. Sci. Eng., B 272 (2021), 115347, https://doi.org/10.1016/j.mseb.2021.115347.
[8] F. Cilia, S.D. Meo, L. Farrugia, J. Bonello, I. Farhat, E.J. Dimech, M. Pasian, C. V. Sammut, Techniques for Temperature-dependent Dielectric Measurements: a Review, Microwave Mediterranean Symposium (MMS), 2022, pp. 1–4, https://doi.org/10.1109/MMS55062.2022.9825550.
[9] M. Saleem, M.S. Butt, A. Maqbool, M.A. Umer, M. Shahid, F. Javaid, R.A. Malik, H. Jabbar, H.M.W. Khalil, L.D. Hwan, M. Kim, B.-K. Koo, S.J. Jeong, Percolation phenomena of dielectric permittivity of a microwave-sintered $BaTiO_3$–Ag nanocomposite for high energy capacitor, J. Alloys Compd. 822 (2020), 153525, https://doi.org/10.1016/j.jallcom.2019.153525.
[10] M.T. Sebastian, H. Jantunen, Low loss dielectric materials for LTCC applications: a review, Int. Mater. Rev. 53 (2) (2008) 57–90, https://doi.org/10.1179/174328008X277524.
[11] L. Wang, J. Yang, W. Cheng, J. Zou, D. Zhao, Progress on polymer composites with low dielectric constant and low dielectric loss for high-frequency signal transmission, Front. Mater. 8 (2021), 774843, https://doi.org/10.3389/fmats.2021.774843.
[12] M.T. Sebastian, R. Ubic, H. Jantunen, Low-loss dielectric ceramic materials and their properties, Int. Mater. Rev. 60 (7) (2015) 392–412, https://doi.org/10.1179/1743280415Y.0000000007.
[13] S.-Z. Hao, D. Zhou, F. Hussain, W.-F. Liu, J.-Z. Su, D.-W. Wang, Q.-P. Wang, Z.-M. Qi, C. Singh, S. Trukhanov, Structure, spectral analysis and microwave dielectric properties of novel $x(NaBi)0.5MoO_4$-$(1-x)Bi_2/3MoO_4$ ($x = 0.2 - 0.8$) ceramics with low sintering temperatures, J. Eur. Ceram. Soc. 40 (2020) 3569–3576, https://doi.org/10.1016/j.jeurceramsoc.2020.03.074.
[14] S.-Z. Hao, D. Zhou, L.-X. Pang, M.-Z. Dang, S.-K. Sun, T. Zhou, S. Trukhanov, A. Trukhanov, A.S.B. Sombra, Q. Li, X.-Q. Zhang, S. Xia, M.A. Darwish, Ultra-low temperature co-fired ceramics with adjustable microwave dielectric properties in

Na_2O-Bi_2O_3-MoO_3 ternary system: a comprehensive study, J. Mater. Chem. C 10 (2022) 2008–2016, https://doi.org/10.1039/D1TC05557G.
[15] V.A. Turchenko, A.V. Trukhanov, I.A. Bobrikov, S.V. Trukhanov, A.M. Balagurov, Study of the crystalline and magnetic structures of $BaFe_{11.4}Al_{0.6}O_{19}$ in a wide temperature range, J. Surf. Investig. 9 (2015) 17–23, https://doi.org/10.1134/S1027451015010176.
[16] M.V. Zdorovets, A.L. Kozlovskiy, D.I. Shlimas, D.B. Borgekov, Phase transformations in FeCo - Fe_2CoO_4/Co_3O_4-spinel nanostructures as a result of thermal annealing and their practical application, J. Mater. Sci. Mater. Electron. 32 (2021) 16694–16705, https://doi.org/10.1007/s10854-021-06226-5.
[17] D. Kaur, A. Bharti, T. Sharma, C. Madhu, Dielectric properties of ZnO-based nanocomposites and their potential applications, Int. J. Optics 2021 (2021), 9950202, https://doi.org/10.1155/2021/9950202.
[18] J. Li, C. Yang, Y. Shan, Y. Lu, C. Li, X. Zhang, H. Zhou, Study on the structure and dielectric properties of BaO-MgONb$_2O_5$-based high-Q ceramic, Mater. Res. Bull. 149 (2022), 111733, https://doi.org/10.1016/j.materresbull.2022.111733.
[19] P. Singh, Preparation and characterization of zinc-barium oxide composite, J. Mater. Sci. Lett. 9 (1990) 613–615, https://doi.org/10.1007/BF00725895.
[20] A.C. Caballero, F.J. Valle, M. Villegas, C. Moure, P. Duran, J.F. Fernandez, Improved chemical stability of ZnO-BaO based varistors, J. Eur. Ceram. Soc. 20 (2000) 2767–2772, https://doi.org/10.1016/S0955-2219(00)00226-0.
[21] A. Srivastava, P. Singh, A. Mitra, Microstructural studies on ZnO-BaO ceramics, Mater. Lett. 5 (1987) 269–275, https://doi.org/10.1016/0167-577X(87)90109-1.
[22] G.N.S. Vijayakumar, Electrical and non-linear optical studies on electrospun ZnO/BaO composite nanofibers, Front. Mater. Sci. 6 (2012) 69–78, https://doi.org/10.1007/s11706-012-0158-4.
[23] N.A. Algarou, Y. Slimani, M.A. Almessiere, F.S. Alahmari, M.G. Vakhitov, D. S. Klygach, S.V. Trukhanov, A.V. Trukhanov, A. Baykal, Magnetic and microwave properties of $SrFe_{12}O_{19}$/$MCe_{0.04}Fe_{1.96}O_4$ (M = Cu, Ni, Mn, Co and Zn) hard/soft nanocomposites, J. Mater. Res. Technol. 9 (2020) 5858–5870, https://doi.org/10.1016/j.jmrt.2020.03.113.
[24] A.L. Kozlovskiy, M.V. Zdorovets, Effect of doping of $Ce^{4+/3+}$ on optical, strength and shielding properties of (0.5-x)TeO_2-0.25MoO-0.25Bi_2O_3-xCeO_2 glasses, Mater. Chem. Phys. 263 (2021), 124444, https://doi.org/10.1016/j.matchemphys.2021.124444.
[25] O.S. Yakovenko, L.Yu Matzui, L.L. Vovchenko, O.V. Lozitsky, O.I. Prokopov, O. A. Lazarenko, A.V. Zhuravkov, V.V. Oliynyk, V.L. Launets, S.V. Trukhanov, A. V. Trukhanov, Electrophysical properties of epoxy-based composites with graphite nanoplatelets and magnetically aligned magnetite, Mol. Cryst. Liq. Cryst. 661 (2018) 68–80, https://doi.org/10.1080/15421406.2018.1460243.
[26] A.V. Trukhanov, D.I. Tishkevich, S.V. Podgornaya, E.Yu Kaniukov, M.A. Darwish, T.I. Zubar, A.V. Timofeev, E.L. Trukhanova, V.G. Kostishyn, S.V. Trukhanov, Impact of the nanocarbon on magnetic and electrodynamic characteristics of the ferrite/polymer composites, Nanomaterials 12 (2022) 868, https://doi.org/10.3390/nano12050868.
[27] R.C.C. Monteiro, A.A.S. Lopes, M.M.A. Lima, J.P. Veiga, R.J.C. Silva, C.J. Dias, E.J. R. Davim, M.H.V. Fernandes, Sintering, crystallization, and dielectric behavior of barium zinc borosilicate glasses-effect of barium oxide substitution for zinc oxide, J. Am. Ceram. Soc. 95 (2012) 3144–3150, https://doi.org/10.1111/j.1551-2916.2012.05418.x.
[28] S. Acharya, J. Torgersen, Y. Kim, J. Park, P. Schindler, A.L. Dadlani, M. Winterkorn, Sh Xu, S.P. Walch, T. Usui, C. Schildknecht, F.B. Prinz, Self-limiting atomic layer deposition of barium oxide and barium titanate thin films using a novel pyrrole based precursor, J. Mater. Chem. C 4 (2016) 1945, https://doi.org/10.1039/C5TC03561A.
[29] F. Ben Messaoud, H. Rahmouni, A. Dhahri, N. Bouguila, J. Dhahria, K. Khirouni, Structural, dielectric and electrical properties of Zn doped $Ba_{0.8}Sr_{0.2}TiO_3$, Ceram. Int. 41 (9/A) (2015) 10910–10914, https://doi.org/10.1016/j.ceramint.2015.05.033.
[30] N.M. Shash, I.S. Ahmed, Structure and electrical properties of ZnO doped barium-metaphosphate glasses, Mater. Chem. Phys. 137/3 (2013) 734–741, https://doi.org/10.1016/j.matchemphys.2012.09.054.
[31] D. Choudhary, S. Sinha, A systematic review on the dielectric response of polyvinyl alcohol - zinc oxide nanocomposites films, J. Phys.: Conf. Ser. 2267 (2022), 012046, https://doi.org/10.1088/1742-6596/2267/1/012046.
[32] A.u.R. Shah, M.N. Prabhakar, M. Saleem, J.-I. Song, Development of biowaste encapsulated polypropylene composites: thermal, optical, dielectric, flame retardant, mechanical, and morphological properties, Polym, Composer 38 (2017) 236–243, https://doi.org/10.1002/pc.23580.
[33] G.-W. Hsieh, L.-C. Shih, P.-Y. Chen, Porous Polydimethylsiloxane elastomer hybrid with zinc oxide nanowire for wearable, wide-range, and low detection limit capacitive pressure sensor, Nanomaterials (Basel) 14 12 (2) (2022) 256, https://doi.org/10.3390/nano12020256.
[34] E.U. Haq, M.R.A. Karim, K.I. Khan, W. Akram, S.S. Hassan, F. Kashi, Study of structural and electrical properties of Zn-doped barium titanate ceramics synthesized by conventional solid-state method, J. Optoelectron. Adv. Mater. 24 (1–2) (2022) 69–73. https://joam.inoe.ro/.
[35] Y. Liu, X.-Y. Zhao, Y.-G. Sun, W.-Z. Li, X.-S. Zhang, J. Luan, Synthesis and applications of low dielectric polyimide, Res. Chem. Mater. (2022), https://doi.org/10.1016/j.recm.2022.08.001.
[36] W. Zhou, Z. Wang, L. Dong, X. Sui, Q. Chen, Dielectric properties and thermal conductivity of PVDF reinforced with three types of Zn particles, Compos. Appl. Sci. Manuf. 79 (2015) 183–191, https://doi.org/10.1016/j.compositesa.2015.09.004.
[37] M. Han, K. Zhao, Dielectric behavior of suspensions of polystyrene-zinc oxide composite microspheres, ACS: J. Phys. Chem. C 112 (25) (2008) 9192–9202, https://doi.org/10.1021/jp8005475.
[38] J. Huang, H. Zheng, Z. Chen, Q. Gao, N. Ma, P. Du, Percolative ceramic composites with giant dielectric constants and low dielectric losses, J. Mater. Chem. 19 (2009) 3909, https://doi.org/10.1039/B820815H.
[39] M. Cao, X.J. Yan, L. Li, S.Y. Wu, X.M. Chen, Obtaining greatly improved dielectric constant in $BaTiO_3$-epoxy composites with low ceramic volume fraction by enhancing the connectivity of ceramic phase, ACS Appl. Mater. Interfaces 14 (5) (2022) 7039–7051, https://doi.org/10.1021/acsami.1c25069.
[40] B.S. –Musialska, D. Szwagierczak, J. Kulawik, N. Pałka, P. Piasecki, Structural, thermal and dielectric properties of low dielectric permittivity cordierite-mullite-glass substrates at terahertz frequencies, Materials 14 (14) (2021) 4030, https://doi.org/10.3390/ma14144030.
[41] X. Chou, J. Zhai, X. Yao, Dielectric tunable properties of low dielectric constant Ba0.5Sr0.5TiO3–Mg2TiO4 microwave composite ceramics, Appl. Phys. Lett. 91 (2007), 122908, https://doi.org/10.1063/1.2784202.
[42] S.V. Trukhanov, A.V. Trukhanov, V.A. Turchenko, An.V. Trukhanov, E. L. Trukhanova, D.I. Tishkevich, V.M. Ivanov, T.I. Zubar, M. Salem, V.G. Kostishyn, L.V. Panina, D.A. Vinnik, S.A. Gudkova, Polarization origin and iron positions in indium doped barium hexaferrites, Ceram. Int. 44 (2018) 290–300, https://doi.org/10.1016/j.ceramint.2017.09.172.
[43] A.L. Kozlovskiy, A. Alina, M.V. Zdorovets, Study of the effect of ion irradiation on increasing the photocatalytic activity of WO_3 microparticles, J. Mater. Sci. Mater. Electron. 32 (2021) 3863–3877, https://doi.org/10.1007/s10854-020-05130-8.
[44] V. Manikandan, A. Vanitha, E.R. Kumar, J. Chandrasekaran, Effect of sintering temperature on Structural and Dielectric properties of Sn substituted $CuFe_2O_4$ Nanoparticles, J. Magn. Magn Mater. 423 (2017) 250–255, https://doi.org/10.1016/j.jmmm.2016.09.077.
[45] M.S. Hamzah, M.W. Wildan, Kusmono, E. Suharyadi, Effect of sintering temperature on physical, mechanical, and electrical properties of nano silica particles synthesized from Indonesia local sand for piezoelectric application, J. Asian Ceram.Soc. 11 (1) (2023) 178–187, https://doi.org/10.1080/21870764.2023.2173851.
[46] J.P. Kumar, K.S.K.R.C. Sekhar, T.D. Rao, P.D. Babu, P. Tirupathi, Effect of sintering temperature on structural, dielectric, and electrical property studies of Bi4NdTi3FeO15 aurivillius ceramics, J. Mater. Sci. Mater. Electron. 32 (2021) 9675–9684, https://doi.org/10.1007/s10854-021-05628-9.
[47] G. He, Z. Li, Y. Dong, G. Wang, Effects of excessive magnesium oxide and sintering regime on microstructure and dielectric properties of forsterite ceramics for millimeterwave dielectrics, J. Mater. Sci. Mater. Electron. 33 (2022) 3129–3138, https://doi.org/10.1007/s10854-021-07515-9.
[48] K. Verma, S. Goel, R. Sharma, Influence of calcination and sintering temperature on the microstructure, dielectric, ferroelectric and piezoelectric properties of the lead-free KNN ceramics, J. Mater. Sci. Mater. Electron. 33 (2022) 26067–26085, https://doi.org/10.1007/s10854-022-09295-2.
[49] Z. Wang, F. Pan, L. Liu, Q. Du, R. Tang, J. Ai, H. Zhang, Y. Chen, Enhanced microwave dielectric properties and sintering behaviors of Mg_2SiO_4-Li_2TiO_3-LiF ceramics by adding $CaTiO_3$ for LTCC and GPS antenna applications, Crystals 12 (4) (2022) 512, https://doi.org/10.3390/cryst12040512.
[50] C.-C. Cheng, T.-E. Hsieh, I.-N. Lin, Microwave dielectric properties of glass-ceramic composites for low temperature co-firable ceramics, J. Eur. Ceram. Soc. 23 (14) (2003) 2553–2558, https://doi.org/10.1016/S0955-2219(03)00166-3.
[51] M. Jebli, C. Rayssi, N.J.D. Abdelmoula, H. Belmabrouk, H. Alrobei, Frequency and thermal studies of dielectric permittivity and Raman analysis of Ba0.97La0.02Ti0.98Nb0.016O3, J. Mater. Sci. Mater. Electron. 31 (2020) 22323–22339, https://doi.org/10.1007/s10854-020-04734-4.
[52] M.A. Ansari, N. Jahan, Structural and optical properties of BaO nanoparticles synthesized by facile Co-precipitation method, Mater. Highlights 2 (2021) 23–28, https://doi.org/10.2991/mathi.k.210226.001.
[53] B. Chouchene, T.B. Chaabane, L. Balan, E. Girot, K. Mozet, G. Medjahdi, R. Schneider, High performance Ce-doped ZnO nanorods for sunlight-driven photocatalysis, Beilstein J. Nanotechnol. 7 (2016) 1338–1349, 10.3762/bjnano.7.125.
[54] A. Saboori, S. Moheimani, M. Pavese, C. Badini, P. Fino, New nanocomposite materials with improved mechanical strength and tailored coefficient of thermal expansion for electro-packaging applications, Metals 7 (2017) 536, https://doi.org/10.3390/met7120536.
[55] J.-M. Oh, J.-G. Koo, J.-W. Lim, Variation in lattice parameters and strain of sintered titanium powder by advanced hydrogen sintering process, Powder Technol. 330 (2018) 27–31, https://doi.org/10.1016/j.powtec.2018.02.018.
[56] B.M. Weckhuysen, Snapshots of a working catalyst: possibilities and limitations of in situ spectroscopy in the field of heterogeneous catalysis, Chem. Commun. 2 (2002) 97–110, 10.1039/B107686H.
[57] M. Silambarasan, S. Saravanan, T. Soga, Raman and photoluminescence studies of Ag and Fe-doped ZnO nanoparticles, Int. J. ChemTech Res. 7 (3) (2015) 1644.
[58] C. Li, X.-M. Wang, Z.-P. Yang, H. Jiao, $Ca_8Mg_7Si_9N_{22}$:Ce^{3+}—a yellow-emitting nitride phosphor for white light emitting diodes, ACS Appl. Electron. Mater. 2 (4) (2020) 936–943, https://doi.org/10.1021/acsaelm.0c00004.
[59] J. Liqiang, Q. Yichun, W. Baiqi, L. Shudan, J. Baojiang, Y. Libin, F. Wei, F. Honggang, S. Jiazhong, Review of photoluminescence performance of nano-sized semiconductor materials and its relationships with photocatalytic activity, Sol. Energy Mater. Sol. Cell. 90 (12) (2006) 1773–1787, https://doi.org/10.1016/j.solmat.2005.11.007.

[60] Y. Song, S. Zhang, C. Zhang, Y. Yang, K. Lv, Raman spectra and microstructure of zinc oxide irradiated with swift heavy ion, Crystals 9 (2019) 395, https://doi.org/10.3390/cryst9080395.
[61] E. Sundharam, A.K.S. Jeevaraj, C. Chinnusamy, Effect of ultrasonication on the synthesis of barium oxide nanoparticles, J. Bionanoscience 11 (4) (2017) 310–314, https://doi.org/10.1166/jbns.2017.1449.
[62] S. Abramowitz, N. Acquista, The infrared spectrum of matrix isolated BaO_2, J. Res. Natl. Bur. Stand. 75 (1971) 23–25, https://doi.org/10.6028/jres.075a.003.
[63] S. Chauhan, R. Kumar, A. Umar, S. Chauhan, G. Kumar, M. Faisal, S.W. Hwang, A. A.-Hajry, Utilization of ZnO nanocones for the photocatalytic degradation of acridine orange, J. Nanosci. Nanotechnol. 11 (5) (2011) 4061–4066, https://doi.org/10.1166/jnn.2011.4166.
[64] M.L.d. S.-Neto, M.C.A.d. Oliveira, C.T. Dominguez, R.E.M. Lins, N. Rakov, C.B. d. Araújo, L.d.S. Menezes, H.P.d. Oliveira, A.S.L. Gomes, UV random laser emission from flexible ZnO-Ag-enriched electrospun cellulose acetate fiber matrix, Sci. Rep. 9 (2019), 11765, https://doi.org/10.1038/s41598-019-48056-w.
[65] E. Roedel, A. Urakawa, S. Kureti, A. Baiker, On the local sensitivity of different IR techniques: Ba species relevant in NO_x storage-reduction, Phys. Chem. Chem. Phys. 10 (40) (2008) 6190, https://doi.org/10.1039/b808529c.
[66] R.H.P. Devamani, M. Alagar, Synthesis and characterization of barium hydroxide nanoparticles, Asian Acad. Res. J. Multidiscip. 1 (23) (2014) 60–75.
[67] G. Panomsuwan, H. Manuspiya, Dielectric properties and discharge energy density of epoxy composites with 3D $BaTiO_3$ network structure, Mater. Lett. 270 (2020), 127695, https://doi.org/10.1016/j.matlet.2020.127695.
[68] A. Chaves, J.G. Azadani, H. Alsalman, D.R. Da Costa, R. Frisenda, A.J. Chaves, S. H. Song, Y.D. Kim, D. He, J. Zhou, A. C-Gomez, F.M. Peeters, Z. Liu, C.L. Hinkle, S.-H. Oh, P.D. Ye, S.J. Koester, Y.H. Lee, Ph Avouris, X. Wang, T. Low, Bandgap engineering of two-dimensional semiconductor materials, npj 2D Mater, Appl 4 (2020) 29, https://doi.org/10.1038/s41699-020-00162-4.
[69] B. Li, Q. Long, D. Duan, Effect of sintering temperatures on properties of $BaO–B_2O_3–SiO_2–Al_2O_3$ glass/silica composites for CBGA package, J. Mater. Sci. Mater. Electron. 27 (2016) 2206–2211, https://doi.org/10.1007/s10854-015-4012-1.
[70] M. Syazwan, R. Azis, M. Hashim, I. Ismayadi, S. Kanagesan, A.N. Hapishah, Co–Ti- and Mn–Ti-substituted barium ferrite for electromagnetic property tuning and enhanced microwave absorption synthesized via mechanical alloying, J. Australas. Ceram. Soc. 53 (2017) 465–474, https://doi.org/10.1007/s41779-017-0056-4.
[71] S.V. Trukhanov, I.O. Troyanchuk, V.V. Fedotova, V.A. Ryzhov, A. Maignan, D. Flahaut, H. Szymczak, R. Szymczak, Magnetic properties of the nonstoichiometric Sr-doped manganites, Phys. Status Solidi 242 (2005) 1123–1131, https://doi.org/10.1002/pssb.200402143.
[72] D.I. Shlimas, A.L. Kozlovskiy, M.V. Zdorovets, Study of the formation effect of the cubic phase of $LiTiO_2$ on the structural, optical, and mechanical properties of $Li_{2\pm x}Ti_{1\pm x}O_3$ ceramics with different contents of the X component, J. Mater. Sci. Mater. Electron. 32 (2021) 7410–7422, https://doi.org/10.1007/s10854-021-05454-z.